Heterostructures of Single-Walled Carbon Nanotubes and Carbide Nanorods

Y. Zhang,[1]* T. Ichihashi,[1] E. Landree,[2] F. Nihey,[1] S. Iijima[1,3]

A method based on a controlled solid-solid reaction was used to fabricate heterostructures between single-walled carbon nanotubes (SWCNTs) and nanorods or particles of silicon carbide and transition metal carbides. Characterization by high-resolution transmission electron microscopy and electron diffraction indicates that the heterostructures have well-defined crystalline interfaces. The SWCNT/carbide interface, with a nanometer-scale area defined by the cross section of a SWCNT bundle or of a single nanotube, represents the smallest heterojunction that can be achieved using carbon nanotubes, and it can be expected to play an important role in the future fabrication of hybrid nanodevices.

Heterostructures with well-defined crystalline interfaces are essential in electronic devices. The prospect of heterostructures made from single-walled carbon nanotubes (SWCNTs) (*1*) are of particular interest for nanodevices because of their useful size scale and their unique electronic properties. SWNTs can be either semiconducting or metallic, depending on their diameter and chirality (*2*). Carbide materials also play an important role in the electronics industry. For example, silicon carbide (SiC) is a useful wide-gap semiconductor for high-temperature, high-frequency, or high-power applications (*3*). Transition metal carbides, such as titanium carbide (TiC) and niobium carbide (NbC), are good metallic conductors with high melting points, high corrosion resistance, and low diffusion coefficients and are therefore suitable for interconnects in ultra-large–scale integrated circuits (*4*). Combining these materials with SWCNTs may open the possibility for new device applications. However, until now there have been no techniques available for fabricating SWCNT/carbide heterojunctions. Earlier investigations have reported a method for fabricating carbide nanorods from multiwalled carbon nanotubes (MWCNTs) through a vapor-solid reaction (*5*). This method has not been used for fabricating nanojunctions because of the difficulty of controlling the reaction region along the carbon nanotube (*6*). Recently, Hu *et al.* have reported a catalytic vapor growth method for fabricating heterojunctions between MWCNTs and Si nanowires (*7*). The electrical characterization has shown the typical rectifying behaviors for the metal-semiconductor junctions produced by this method. However, the need for specific catalysts and vapor reactants has limited the generality of the method and caused several demerits. The first demerit is the presence of catalyst clusters at or near the junctions produced by growing MWCNTs on Si nanowires. The second is the contamination of amorphous Si and SiO_x layers on the surfaces of both nanotubes and nanowires while growing Si nanowires on the MWCNTs. The third is the unexpected doping of catalyst atoms in Si nanowires. These demerits have made it difficult to obtain a sharply defined interface and may influence the structure and properties of a junction with a smaller size, such as an individual SWCNT junction.

In this report, we describe a simple and clean method for fabricating SWCNT/carbide heterostructures with well-defined nanometer-scale interfaces. The method is based on a direct solid-solid reaction: C (nanotubes) + M (solid) → MC (solid), where M is either Si or a transition metal. The reaction is spatially restricted by partial contact between the surface of the solid reactant (M) and carbon nanotubes and by performance of the reaction in ultra-high vacuum or an inert atmosphere to avoid any volatile reactant. The carbide initially forms at the C/M interface once a sufficient temperature (T) is reached for the reaction to occur (roughly $T > 800$°C) (Fig. 1). The continuous transformation of the SWCNTs to carbide is controlled by the diffusion of M to the C/MC interface (*8*). However, the self-diffusion rate through bulk SiC or transition metal carbide is extremely slow in the temperature range of interest ($800°C < T < 1000°C$). A continuous supply of Si or metal atoms is therefore transported primarily via surface diffusion. This is consistent with the known formation of SiC films on the surface of Si (*8*). The diffusion path length, along with the annealing temperature and time, provide a means of controlling the formation of the SWCNT/MC heterostructure near the site of the contact between SWCNTs and the M substrate.

Samples for structure investigation were prepared by thinning Si, Ti, and Nb substrates with perforations by means of conventional transmission electron microscopy (TEM) sample preparation techniques (*9*). SWCNTs produced by laser ablation (*10*) were dispersed in ethanol and then deposited on the prepared substrate. Long, highly curved, and interconnected SWCNT bundles (*11*) formed a three-dimensional structure on the surface of the substrate after the ethanol had evaporated. This resulted in partial contact of SWCNTs with Si or metal surfaces (*12*). The prepared specimens were then heated in the ultra-high–vacuum TEM column or in a side chamber either by an infrared heating lamp or by electrical current heating of the substrate. The maximum substrate temperature was measured with an optical pyrometer to be 970°C. Each sample was heated for about 20 min.

Investigation of the SWCNTs dispersed on Si showed signs of Si surface migration during heating in TEM (*13*). Silicon diffusion along the SWCNT bundles resulted in the formation of long SiC nanorods near the specimen perforation edge (Fig. 2A). The curved nanorods have a similar morphology to that of the SWCNT bundles from which they were made (*11*). Unreacted SWCNTs connected with the formed SiC nanorods were found dispersed throughout the thin specimen. The reaction in the thin substrate region is mainly restricted by a locally insufficient supply of Si. After the nearby Si has been transformed into SiC, the diffusion distance of Si to the C/SiC interface increases rapidly. Figure 2B shows well-separated reacted and unreacted regions. The unreacted SWCNTs far from the Si substrate retained their morphology as described in (*10*). An electron diffraction pattern (Fig. 2B, inset) from the reacted region verified the formation of β-phase SiC (*14*).

Most SWCNT bundles are joined to crystallized SiC nanorods (Fig. 2, C and D). Individual SWCNTs or bundles consisting of only a small number of SWCNTs are usually joined to SiC nanoparticles rather than nanorods (Fig. 2, E and F). The SWCNT/SiC interfaces appeared well ordered, without evidence for any amorphous phase. The lattice image in Fig. 2D clearly shows <110> projection of two sets of {111} planes of β-SiC with a plane spacing of ~0.25 nm. These nearly ideal heterostructures represent a new kind of nanometer-scale molecule/crystal interface. From the models of the heterostruc-

[1]Fundamental Research Laboratories, NEC Corporation, 34 Miyukigaoka, Tsukuba, Ibaraki 305-8501, Japan. [2]Department of Materials Science and Engineering, Northwestern University, 2225 North Campus Drive, Evanston, IL 60208, USA. [3]Japan Science and Technology Corporation, c/o Department of Physics, Meijo University, 1-501 Shiogamaguchi, Tenpaku-ku, Nagoya 468-8502, Japan.

*To whom correspondence should be addressed. E-mail: zhang@frl.cl.nec.co.jp

tures shown in Fig. 2, E and F (Fig. 2, G and H, respectively), we can estimate the interface area, which is determined by the total cross-section area of adjacent SWCNTs. The diameter of the SWCNT is about 1.3 nm, and thus the cross-section area of a single SWCNT is about 1.3 nm^2 and that of a five-tube bundle is about 6.5 nm^2. At this scale, the behavior of the interface is strongly influenced by the detailed configuration of interfacial atoms. This is more pronounced in the case of a carbon nanotube because of its low atomic density. A single (10, 10) SWCNT will contribute only 20 interfacial atoms in an ideal case (*15*). In practice, the number and configuration of the interfacial atoms are determined by the nanotube chirality and diameter, the crystal orientation of SiC relative to the interface, and the relaxation structure due to the lattice mismatch between the SiC surface and the nanotube cross section.

An investigation of SWCNTs dispersed on Ti produced comparable results under similar processing conditions. Many SWCNT/TiC heterostructures were observed upon annealing, as was the formation of nanorod-like TiC (Fig. 3). The difference between the nanorod morphology shown in Fig. 3A and that in Fig. 2A is attributed to the different diffusion rate of Ti and Si. A selected-area electron diffraction pattern (Fig. 3B, inset) indicates the formation of NaCl-structured TiC. The limited thickness of the TiC layer formed on the surface of the amorphous carbon cluster (Fig. 3B) is a result of the very low bulk diffusion coefficient and of a locally insufficient supply of Ti. In general, the surface diffusion along the length of the SWCNTs is much larger than bulk diffusion, and thus complete reaction in the radial direction of SWCNT bundles could only occur in bundles of relatively small diameter with a limited number of SWCNTs (Fig. 3, C and E). Bundles with a large diameter or those covered by a thick amorphous carbon layer resulted in the presence of unreacted SWCNTs at the center of the partially carbonized bundle (Fig. 3D). In the TEM image of Fig. 3D, residual SWCNTs inside the void can be clearly seen. It should be noted that incomplete reaction at centers of very large bundles was also found in SWCNT-Si specimens. However, the void formation in SiC is not as pronounced as in TiC, because the reaction temperature is close to the melting point of Si, and Si has a higher self-diffusion rate in SiC than Ti has in TiC.

Niobium has a much higher melting point than Si and Ti, and thus a much lower diffusion coefficient (*16*). This might explain why

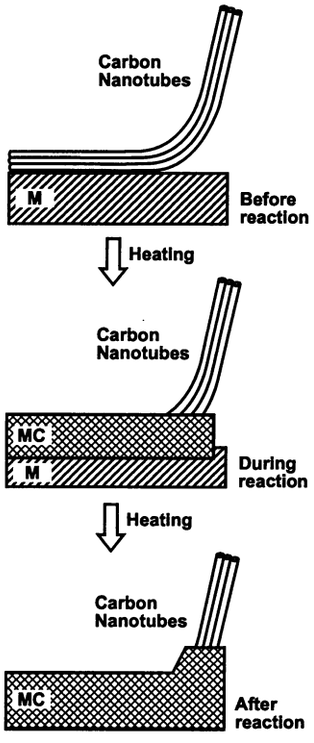

Fig. 1. A schematic illustration of the method for fabricating nanotube/carbide heterostructures by means of a solid-solid reaction. The top drawing shows a partial contact between the solid reactant (M = Si or transition metals) and carbon nanotubes. The middle drawing shows the formation of carbide (MC) near the point of contact by diffusive reaction during heating. The bottom drawing shows the growth of a nanorod and the formation of a nanojunction when the growth stops under the limitation of reaction time or M supply. The residual M source is not shown in the bottom drawing.

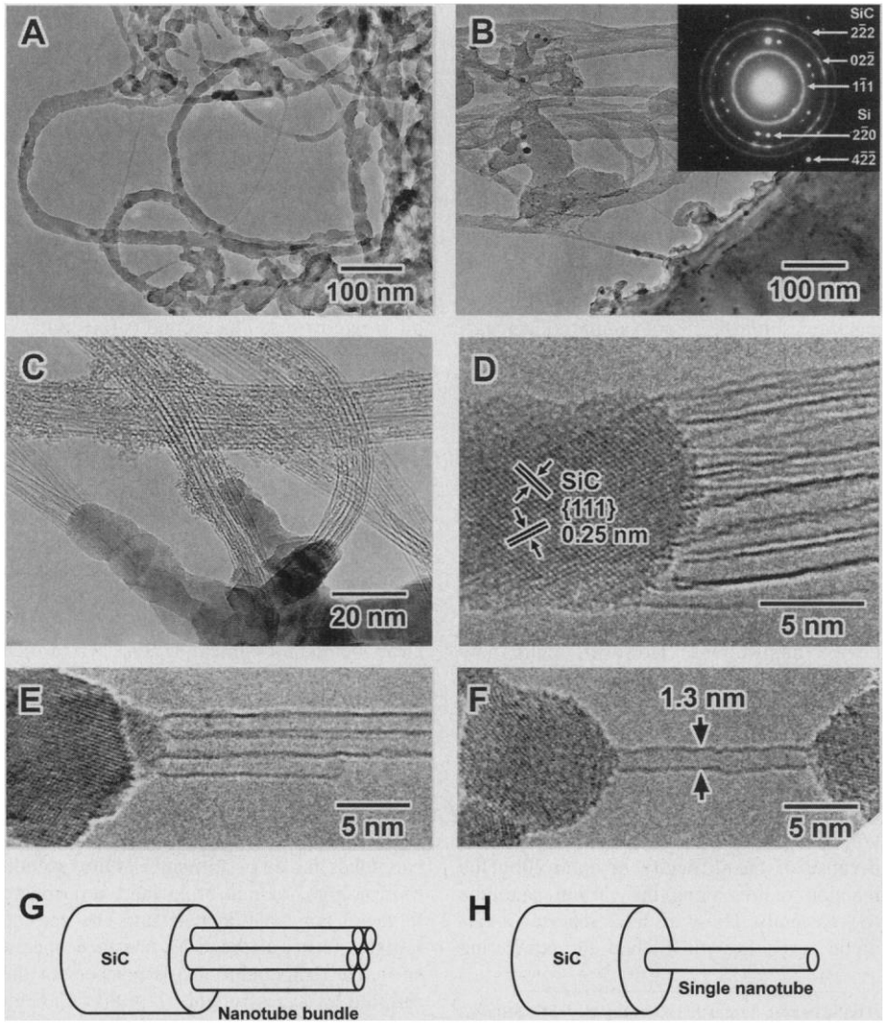

Fig. 2. (**A**) TEM image showing SiC nanorods and SWCNT bundles connected by the nanorods. (**B**) TEM image showing SWCNTs far from the Si substrate (top left) and the reacted substrate (bottom right) after heating. The inset shows an electron diffraction pattern taken from the reacted substrate. (**C** and **D**) High-resolution TEM images showing heterostructures between SWCNT bundles and SiC nanorods. The lattice image in (D) clearly shows two sets of {111} planes (spacing is ~0.25 nm) of β-SiC with the <110> axis parallel to the electron beam. (**E**) Interfaces between SiC and a bundle consisting of five SWCNTs and (**F**) between SiC and a single SWCNT. (**G**) and (**H**) are models of the heterostructures shown in (E) and (F), respectively.

no rodlike NbC formation was observed along SWCNTs under the same processing conditions. Only a few SWCNT bundles were found connected directly with the NbC matrix. Most of them broke at the interface, possibly during cooling of the specimen. We often found NbC nanocrystal particles attached to the ends of broken SWCNT bundles.

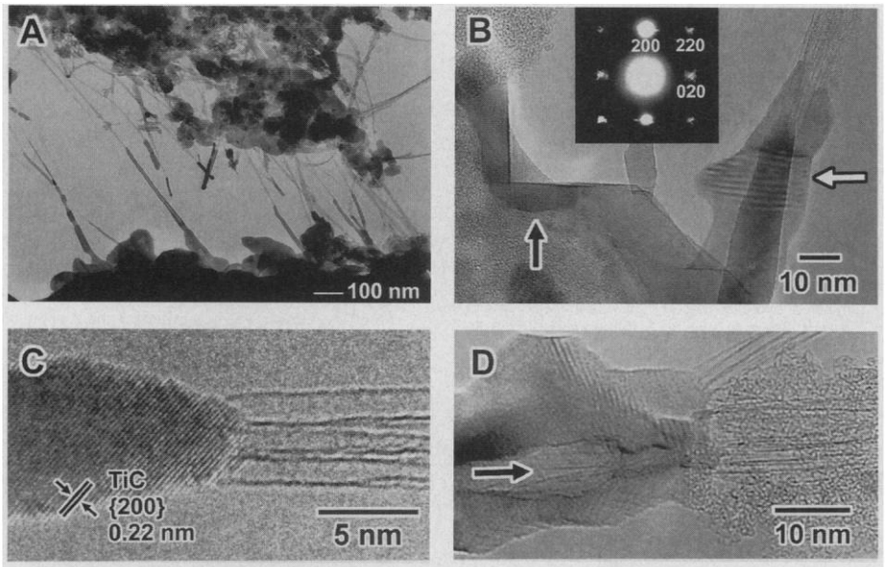

Fig. 3. (**A**) TEM image showing SWCNT bundles connected with rodlike TiC sticking out of the reacted substrate (bottom). (**B**) TEM image of two overlapping nanorods (white arrow) and their electron diffraction pattern (inset). A TiC layer on the surface of an amorphous carbon cluster is also shown (black arrow). (**C**) High-resolution TEM image of an interface between TiC and a SWCNT bundle. The lattice fringes of TiC represent {200} planes with a spacing of ~0.22 nm. (**D**) TEM image showing void formation in TiC. The line contrast inside the void indicates residual SWCNTs (arrow). (**E**) High-resolution TEM image of a heterostructure between a single SWCNT and an elongated TiC particle. The lateral size of the TiC particle is similar to that of a SWCNT (<2 nm). The lattice fringes of TiC represent {111} lattice planes (spacing ~0.25 nm).

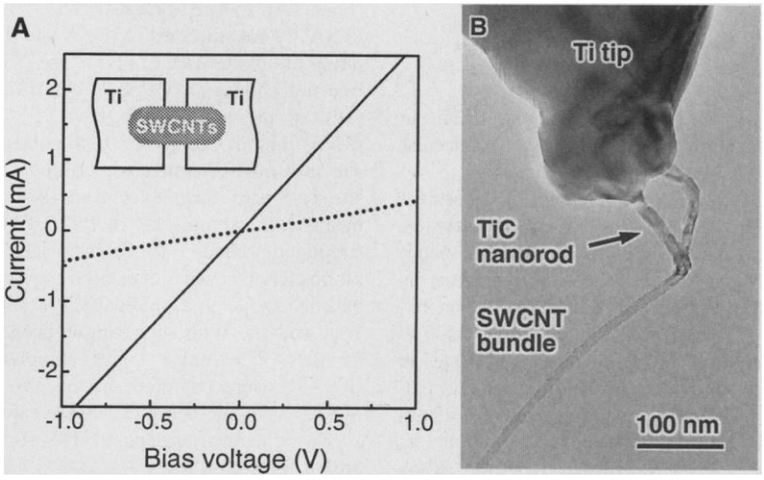

Fig. 4. (**A**) *I-V* curves of a SWCNT matrix bridging two Ti pads (as illustrated in the inset) before (dotted line) and after (solid line) final annealing. The gap between the two pads is 50 μm. The absolute resistance values in the measurements are dependent on the amount of SWCNTs and the contact area with the Ti pads. All the experiments (>10) show that resistance after final annealing decreased to about one-fifth to one-third of the values before annealing. This is mainly attributed to the improvement of electrical contacts. (**B**) TEM image of a SWCNT bundle welded on a Ti-made STM tip through the formation of TiC nanorods. The SWCNT bundle was first mounted on the Ti tip by a micromanipulator in a scanning electron microscope and then was heat-treated under the conditions described here. The formation of two nanorods near the contact point with the Ti tip is caused by a splitting of the bundle before heating.

This technique can easily be extended to connect carbon nanotubes, both single- and multiwalled, to other materials. The electrical transport property of a heterostructure is dependent on the material to which the nanotubes are connected. For metallic SWCNT bundles, a junction with semiconductor (SiC) may result in a Schottky diode, and a junction with transition metal carbide may result in a low-resistance ohmic contact. As an example, we made such ohmic contacts between a SWCNT matrix and Ti pads. An array of Ti pads was deposited on a sapphire substrate by photolithography. The Ti pads were annealed under the same conditions as those described here. Filaments consisting of SWCNT bundles were then deposited in the gaps between Ti pads and were annealed again under the same conditions. Electrical measurements showed that the resistance between two Ti pads connected by SWCNT filaments decreased dramatically after the final treatment, and the current-voltage (*I-V*) characteristics showed a linear behavior (Fig. 4A).

The method described here is not only simple and effective but also highly controllable. Combining this method with a nanomanipulation technique, we welded an individual SWCNT bundle onto a Ti-made scanning tunneling microscope (STM) tip (Fig. 4B). The formed heterostructures were very robust. We found that some of them could survive a blast from an air gun and 1-min ultrasonicating in ethanol. Such heterostructures could be used as robust and conductive carbon nanotube STM probes. A similar manipulation was also successfully applied to a Si tip. By controlling the contact of nanotubes with the solid reactant surface by means of nanomanipulation and an improved heating method, it may be possible to fabricate heterojunctions directly on semiconductor wafers and to hybridize nanotubes into electronic devices.

References and Notes

1. S. Iijima, *Nature* **354**, 56 (1991); S. Iijima and T. Ichihashi, *ibid.* **363**, 603 (1993).
2. M. S. Dresselhaus, G. Dresselhaus, P. Eklund, *Science of Fullerenes and Carbon Nanotubes* (Academic Press, New York, 1996). Experimental verification using STM has been reported recently [J. W. G. Wildàer, L. C. Venema, A. G. Rinzler, R. E. Smalley, C. Dekker, *Nature* **391**, 59 (1998); T. W. Odom, J.-L. Huang, P. Kim, C. M. Lieber, *ibid.*, p. 62].
3. G. L. Harris, Ed., *Properties of Silicon Carbide* (INSPEC, Institution of Electrical Engineers, London, 1995).
4. W. S. Williams, *J. Mater.* **49** (no. 3), 38 (1997); L. E. Toth, *Transition Metal Carbides and Nitrides* (Academic Press, New York and London, 1971).
5. H. Dia, E. W. Wong, Y. Z. Lu, S. Fan, C. Lieber, *Nature* **375**, 769 (1995); D. Zhou, S. Seraphin, *Chem. Phys. Lett.* **222**, 233 (1994); W. Han *et al.*, *ibid.* **265**, 374 (1997).
6. Ideally, the ends of open nanotubes are more reactive than the walls, and thus a vapor-solid reaction could occur preferentially at nanotube ends to form a nanotube/carbide heterojunction at a precisely controlled temperature. However, nanotubes actually produced

contain defects and contamination by amorphous carbon along the length of their walls, which can act as preferential sites for carbonizing to occur.
7. J. Hu, M. Ouyang, P. Yang, C. M. Lieber, *Nature* **399**, 48 (1999).
8. The growth mechanism is inferred from a series of studies of the formation of SiC films on Si substrates, using hydrocarbon or C_{60} carbonization methods that showed that the growth of SiC after nucleation happened at the C/SiC interface rather than the SiC/Si interface [J. Graul and E. Wagner, *Appl. Phys. Lett.* **21**, 67 (1972); C. J. Mogab and H. J. Leamy, *J. Appl. Phys.* **45**, 1075 (1974); J. P. Li and A. J. Steckl, *J. Electrochem. Soc.* **142**, 634 (1995); A. V. Hamza, M. Balooch, M. Moalem, *Surf. Sci.* **317**, L1129 (1994); D. Chen, R. Workman, D. Sarid, *ibid.* **344**, 23 (1995); L. Moro *et al.*, *J. Appl. Phys.* **81**, 6141 (1997); L. Moro *et al.*, *Appl. Surf. Sci.* **119**, 76 (1997)].
9. To prepare the Si specimen, a <111> crystalline Si substrate was thinned by a dimple grinder from a thickness of about 450 μm to several tens of microns at the center. It was further thinned to perforation by chemical etching in a mixed solution with a ratio of $HF:HNO_3$ = 1:4. The thickness near the wedge-shaped perforation edge was less than several tens of nanometers. The oxide film on the Si surface was also removed by the chemical etching. To prepare Ti and Nb specimens, thin foils (thickness ~2 μm) were thinned to perforation by ion milling.
10. The SWCNTs were produced by laser ablation of a graphite target containing 1.2 atomic % of a nickel and cobalt mixture. For a detailed description of the laser ablation method, see (*11*) and T. Guo, P. Nikolaev, A. Thess, D. T. Colbert, R. E. Smalley, *Chem. Phys. Lett.* **243**, 49 (1995).
11. Y. Zhang and S. Iijima, *Philos. Mag. Lett.* **78**, 139 (1998).
12. Strictly speaking, the Si surface as prepared will be terminated by hydrogen or covered with a few monolayers of other surface contaminants, including amorphous carbon, left over from the ethanol used to suspend the SWCNTs. However, these would not influence the result of the experiment, because the surface-terminated hydrogen desorbs at ~500°C [J. Schmidt, M. R. C. Hunt, P. Miao, R. E. Palmer, *Phys. Rev. B* **56**, 9918 (1997)], and the amorphous carbon contamination on the surface of Si forms epitaxial SiC at ~800°C [J. P. Becker, R. G. Long, J. E. Mahan, *J. Vac. Sci. Technol.* **A12**, 174 (1994); R. C. Henderson, R. B. Marcus, W. J. Polito, *J. Appl. Phys.* **42**, 1208 (1971)].
13. A JEM-2000FXVII microscope, with a vacuum of about 10^{-9} torr, was used for the heating experiments and for high-resolution microscopy.
14. The bright spots in the SiC {220} ringlike diffraction pattern indicate a partially epitaxial growth of SiC in a relatively thick Si region. The existence of unreacted Si is also indicated in the same diffraction pattern. The splitting of Si {220} diffraction spots is due to the deformation of the Si substrate during heating.
15. An achiral (10, 10) SWCNT has a diameter close to that indicated by the experimental data. For an explanation of the chiral vector of a nanotube, see (*4*).
16. Bulk self-diffusion parameters for TiC and NbC can be found in G. V. Samsonov and I. M. Vinitskii, *Handbook of Refractory Compounds* (IFI/Plenum, New York, 1980), pp. 222–223.
17. Partially supported by the Special Coordination Funds of the Science and Technology Agency of the Japanese Government. E.L. acknowledges the support of L. D. Marks.

26 April 1999; accepted 20 July 1999

Recognition of the Codon-Anticodon Helix by Ribosomal RNA

Satoko Yoshizawa, Dominique Fourmy, Joseph D. Puglisi*

Translational fidelity is established by ribosomal recognition of the codon-anticodon interaction within the aminoacyl–transfer RNA (tRNA) site (A site) of the ribosome. Experiments are presented that reveal possible contacts between 16*S* ribosomal RNA and the codon-anticodon complex. N1 methylation of adenine at position 1492 (A1492) and A1493 interfered with A-site tRNA binding. Mutation of A1492 and A1493 to guanine or cytosine also impaired A-site tRNA binding. The deleterious effects of A1492G or A1493G (or both) mutations were compensated by 2′fluorine substitutions in the mRNA codon. The results suggest that the ribosome recognizes the codon-anticodon complex by adenine contacts to the messenger RNA backbone and provide a mechanism for molecular discrimination of correct versus incorrect codon-anticodon pairs.

The fidelity of protein synthesis is determined by the interaction of an mRNA codon with the anticodon of the correct (cognate) transfer RNA (tRNA) within the aminoacyl-tRNA site (A site) of the ribosome. The ribosome distinguishes the correct codon-anticodon pair from all noncognate pairs. Despite the relatively low specificity of the codon-anticodon interaction, the measured fidelity of translation is about one error per 10^4 amino acids (*1*). The ribosome achieves high fidelity through a kinetic discrimination mechanism that couples codon-anticodon recognition on the ribosome with hydrolysis of guanosine triphosphate by elongation factor Tu (*2*). Rate constants for tRNA binding to the ribosomal A site are tuned by formation of a cognate or noncognate codon-anticodon pair (*3*). These processes suggest ribosomal recognition of the codon-anticodon pair within an active site for decoding (*4*). The molecular basis of this recognition is not known.

Highly conserved regions of ribosomal RNA (rRNA) form the tRNA-binding sites (*5*). The codon-anticodon interactions in the peptidyl-tRNA site (P site) and A site occur on the small (30*S*) ribosomal subunit (*6*). Fewer nucleotides, located primarily within the 1400 to 1500 region of rRNA, have been implicated in A-site tRNA binding than in P-site tRNA binding (*6*). This agrees with the affinity of a cognate tRNA for the A site being one-fiftieth that for the P site. RNA mutations in 16*S* rRNA affect the fidelity of translation (*5*), and aminoglycoside antibiotics that decrease the fidelity of translation (*7*) bind to 16*S* rRNA and perturb rRNA structure (*8*). These data suggest that the ribosome recognizes the codon-anticodon complex within a defined region of 16*S* rRNA in the 30*S* subunit.

Here, we describe experiments that map possible molecular contacts between 16*S* rRNA and the mRNA-tRNA complex in the A site. Chemical modification interference identified A1492 and A1493 in 16*S* rRNA as required for mRNA-dependent tRNA binding in the A site. Mutations of these two universally conserved nucleotides are lethal in *Escherichia coli* and decrease A-site binding affinity. The deleterious effects of A to G changes at these positions are compensated by 2′F modifications in the mRNA codon. The results support a model for ribosomal decoding in which A1492 and A1493 recognize the helical structure of cognate codon-anticodon complexes in the A site.

A selection scheme was developed to identify bases in 16*S* rRNA whose chemical modification disrupts A-site tRNA binding (Fig. 1A) (*9*). 3′-biotin-$tRNA^{Phe}$ (biotin-$tRNA^{Phe}$) was directed to the A site by saturating the P site with *E. coli* $tRNA^{fMet}$ at the first two codons of phage T4 gene32 mRNA (*10*). In the absence of $tRNA^{fMet}$, biotin-$tRNA^{Phe}$ binds exclusively to the ribosomal P site in a mRNA-dependent fashion (*11*). A-site or P-site complexes were isolated by means of capture of biotin-$tRNA^{Phe}$ by streptavidin beads (*10*). Specific selection of biotin-$tRNA^{Phe}$ was revealed by toeprint experiments (*12*) on captured 30*S* subunits (Fig. 1, A and B). With saturating concentrations of $tRNA^{fMet}$, only A-site complexes of $tRNA^{Phe}$ were captured; in the absence of $tRNA^{fMet}$, P-site complexes were captured.

The chemical groups in 16*S* rRNA required for high-affinity A-site tRNA binding to 30*S* subunits were identified with this selection scheme. 30*S* subunits that were competent for A-site or P-site biotin-$tRNA^{Phe}$ binding after chemical modification were captured with streptavidin beads (*10*, *13*). Comparison of the modification levels of all bases in 16*S* rRNA in the total population and in the bound fraction of 30*S* subunits revealed critical bases for A-site tRNA binding. Only

Department of Structural Biology, Stanford University School of Medicine, Stanford, CA 94305–5126, USA.

*To whom correspondence should be addressed. E-mail: puglisi@stanford.edu